THE JOURNAL OF BIOLOGICAL CHEMISTRY VOL. 281, NO. 49, pp. 37594–37602, December 8, 2006

Tuning of a Neuronal Calcium Sensor*

Received for publication, April 18, 2006, and in revised form, September 29, 2006 Published, JBC Papers in Press, October 2, 2006, DOI 10.1074/jbc.M603700200

Oliver H. Weiergräber[‡1], Ivan I. Senin[§1], Eugene Yu Zernii[§], Valeriya A. Churumova[§¶], Nadezhda A. Kovaleva[§], Aliya A. Nazipova[‖], Sergei E. Permyakov[‖], Eugene A. Permyakov[‖], Pavel P. Philippov[§], Joachim Granzin[‡], and Karl-Wilhelm Koch[2]**

*From the [‡]Institut für Biologische Informationsverarbeitung (IBI-2, Biologische Strukturforschung), Forschungszentrum Jülich GmbH, D-52425 Jülich, Germany, the [§]A. N. Belozersky Institute of Physico-Chemical Biology and the [¶]Faculty of Bioengineering and Bioinformatics, M. V. Lomonosov Moscow State University, 119992 Moscow, Russia, the [‖]Institute for Biological Instrumentation of the Russian Academy of Sciences, Pushchino, Moscow Region 142290, Russia, and the **AG Biochemie, Fakultät V, IBU, Carl-von-Ossietzky-Universität Oldenburg, D-26111 Oldenburg, Germany*

Recoverin is a Ca^{2+}-regulated signal transduction modulator expressed in the vertebrate retina that has been implicated in visual adaptation. An intriguing feature of recoverin is a cluster of charged residues at its C terminus, the functional significance of which is largely unclear. To elucidate the impact of this segment on recoverin structure and function, we have investigated a mutant lacking the C-terminal 12 amino acids. Whereas in myristoylated recoverin the truncation causes an overall decrease in Ca^{2+} sensitivity, results for the non-myristoylated mutant indicate that the truncation primarily affects the high affinity EF-hand 3. The three-dimensional structure of the mutant has been determined by x-ray crystallography. In addition to significant changes in average coordinates compared with wild-type recoverin, the structure provides strong indication of increased conformational flexibility, particularly in the C-terminal domain. Based on these observations, we propose a novel role of the C-terminal segment of recoverin as an internal modulator of Ca^{2+} sensitivity.

Many biological processes are triggered or regulated by transient intracellular Ca^{2+} signals. Because these signals elicit specific cellular responses, the precise detection of changes in cytoplasmic Ca^{2+} concentration is a crucial step in many signaling pathways and requires sensing of Ca^{2+} within very different concentration ranges. Ca^{2+}-binding proteins work as intracellular Ca^{2+} sensors and regulate their targets with high specificity and high spatial and temporal resolution. To achieve these remarkable tasks, Ca^{2+} is recognized by specific amino acid sequence motifs, for example the C_2 domain and the EF-hand motif (1, 2). These motifs can detect subtle changes in Ca^{2+} concentration and allow a fine tuning of Ca^{2+} signaling. However, it remains a challenging problem to understand at a structural level how minimal changes in cytoplasmic Ca^{2+} are reliably detected.

The EF-hand superfamily of Ca^{2+}-binding proteins includes, among others, the family of neuronal calcium sensor (NCS)[3] proteins (3), which are named because of their predominant expression in neuronal tissue. NCS proteins are grouped into five subfamilies and show a rather heterogeneous localization and function in the nervous system (4). In the photoreceptor cells of the vertebrate retina, for instance, recoverin and several isoforms of guanylate cyclase activating protein (GCAP) detect changes in Ca^{2+} concentration during or after illumination and regulate their target proteins in Ca^{2+}-dependent feedback loops (5).

Recoverin inhibits rhodopsin kinase at high cytoplasmic Ca^{2+} concentration (6–9), a process that is thought to contribute to light adaptation of photoreceptor cells (9, 10). Recoverin harbors a myristoyl group at its N terminus (11), which is buried in a hydrophobic cleft in the Ca^{2+}-free state (12). Upon Ca^{2+} binding to the two functional EF-hands (EF-hand 2 and EF-hand 3) (13) the acyl chain is exposed to the solvent. This so-called Ca^{2+}-myristoyl switch is a multistep process, in which the EF-hands are sequentially filled by Ca^{2+} and recoverin undergoes a major conformational change (14–17). Interaction of recoverin with membranes occurs with low to moderate affinity and therefore appears to be driven mainly by hydrophobic forces (17, 18). On the other hand, recoverin contains a remarkable cluster of basic residues at its C terminus, which have been suggested to provide the positive charges for an electrostatic interaction with the membrane (19). Recently, solid state NMR studies on myristoylated recoverin attached to phospholipid bilayers revealed that the positive charges at the C terminus do not make contact with the membrane (20). This apparent discrepancy could be resolved by assuming that the positively charged C terminus does not influence the membrane binding *per se*, but controls the Ca^{2+} binding character-

* This work was supported in part by grants from the Deutsche Forschungsgemeinschaft (to K.-W. K.) (Ko 948/6-1), INTAS (03-51-4548) (to I. I. S., K.-W. K. and P. P. P.), the Ludwig Institute for Cancer Research (to P. P. P.), Russian Foundation for Basic Research (to I. I. S.; 03-04-48909, 06-04-48761) and (to P. P. P.; 04-04-04001, 03-04-49181, 06-04-48018), and by a grant from the Program Molecular and Cellular Biology of the Russian Academy of Sciences. The costs of publication of this article were defrayed in part by the payment of page charges. This article must therefore be hereby marked "*advertisement*" in accordance with 18 U.S.C. Section 1734 solely to indicate this fact.

The atomic coordinates and structure factors (code 2HET) have been deposited in the Protein Data Bank, Research Collaboratory for Structural Bioinformatics, Rutgers University, New Brunswick, NJ (http://www.rcsb.org/).

[1] Both authors contributed equally to this work.

[2] To whom correspondence should be addressed. Tel.: 49-441-7983640; Fax: 49-441-193640; E-mail: karl.w.koch@uni-oldenburg.de.

[3] The abbreviations used are: NCS, neuronal calcium sensor; CBL, calcineurin B-like protein; CIPK, CBL-interacting protein kinase; CN, calcineurin; GCAP, guanylate cyclase activating protein; KChIP, potassium channel interacting protein; ROS, rod outer segment; SPR, surface plasmon resonance; PDB, Protein Data Bank.

istics of the EF-hands. Consequently, all Ca^{2+}-dependent properties of recoverin would depend on the presence of this portion of the protein.

In the present study, we address the impact of the charged C-terminal segment on structure and function of recoverin. To this end, we have determined the crystal structure of a truncated mutant lacking the C-terminal cluster of charged residues and compared it with available structures of wild-type recoverin (12, 15, 16, 21, 22). Furthermore, we have investigated key biochemical properties of the mutant, such as Ca^{2+} binding, association with rod outer segment (ROS) membranes and inhibition of rhodopsin kinase. Based on these data, we propose a novel function of the C terminus of recoverin as an internal modulator of EF-hand function.

EXPERIMENTAL PROCEDURES

Protein Expression and Purification—The expression construct for the truncated bovine recoverin mutant Rc^{2-190} was generated by site-directed mutagenesis using the following oligonucleotide primers: 5′-TAATACGACTCACTATAGGG-3′ and 5′-CTCCTTGGATCCTTAAGGCTCGAATTG-3′ (containing stop codon and BamHI restriction site). The DNA fragment was inserted between the NcoI and BamHI sites of a pET-11d plasmid vector. The integrity of the insert was checked by sequencing using an ABI PRISM 3100-Avant genetic analyzer.

Heterologous expression and purification of all myristoylated and non-myristoylated recoverin variants was performed and analyzed as described previously (17). When necessary, recoverin forms were further purified by reversed phase high performance liquid chromatography using a Vydac 238TP C18 column (4.6 × 250 mm) to obtain homogeneous myristoylated forms of wild type and mutant recoverin. Denatured protein (after elution from a reverse phase column) was refolded as described previously (23).

$^{45}Ca^{2+}$ Binding Assay—Binding of $^{45}Ca^{2+}$ to recoverin was investigated as described previously (17). In summary, 43 μM protein was dissolved in 20 mM Tris-HCl, pH 7.5, 100 mM NaCl and 1 mM dithiothreitol and transferred to Centricon 10 devices (Amicon). Radioactive $^{45}CaCl_2$ was added, the samples were centrifuged for 1 min (5000 rpm, tabletop centrifuge Biofuge pico, Heraeus) and radioactivity of the filtrate was counted (free Ca^{2+}). Next, non-radioactive $CaCl_2$ was added, and the centrifugation procedure was repeated. Protein-bound Ca^{2+} *versus* free Ca^{2+} was determined from the excess Ca^{2+} in the protein sample over that present in the ultrafiltrate. Data were analyzed as described (17).

Equilibrium Centrifugation Assay—Binding of recoverin to ROS membranes was investigated according to a published procedure (14, 17). Briefly, 30 μM recoverin was mixed with bleached urea-washed ROS membranes (50 μM rhodopsin) and incubated at 30 °C (Gnom, DNA-technology thermomixer, 1000 rpm) for 15 min in 20 mM Tris-HCl (pH 7.5), 100 mM NaCl, 20 mM $MgCl_2$, 1 mM DTT, 3 mM BAPTA and 0–50 mM $CaCl_2$ (total volume 75 μl). Membranes were separated by centrifugation (15 min, 14,000 rpm, Heraeus tabletop centrifuge), and the supernatant was removed. The pellet was analyzed by SDS-PAGE.

Surface Plasmon Resonance (SPR) Measurements—Binding of recoverin variants to immobilized liposomes was monitored by SPR spectroscopy. The immobilization of liposomes on sensor chip surfaces, recording of suitable controls and evaluation of SPR data have been described in detail (17, 18).

Fluorescence Measurements—Thermal stability of recoverin variants was studied by recording the wavelength maximum (λ_{max}) of tryptophan fluorescence emission at different temperatures essentially as described before (13). Measurements were performed on a Cary Eclipse spectrofluorimeter (Varian Inc.), equipped with a Peltier-controlled cell holder. All spectra were corrected for the spectral sensitivity of the instrument and fitted to log-normal curves. Positions of λ_{max} were obtained from these fits. Spectrofluorometric temperature scans were performed stepwise allowing the sample to equilibrate at each temperature. The average heating rate was 0.5 °C/min. Temperature was monitored inside the cuvette. Protein concentration was 7–15 μM. Measurements were made in 10 mM Hepes-KOH, pH 8.0 in the presence of either 1 mM $CaCl_2$ or 1 mM EDTA. Excitation wavelength was set to 280 nm.

Rhodopsin Kinase Assay—The kinase assay was performed as described before (22). Briefly, the assay mixture in a final volume of 50 μl contained 10 μM rhodopsin (urea-washed ROS), 20 mM Tris-HCl (pH 7.5), 2 mM $MgCl_2$, 1 mM [γ^{32}P]ATP (30–100 dpm/pmol), 1 mM dithiothreitol, 1 mM phenylmethylsulfonyl fluoride, and 0.3–0.5 units of rhodopsin kinase. The respective recoverin variant and a Ca^{2+}/bisaminobromo-phenoxyethane tetraacetate (BAPTA) buffer were added, as appropriate (17). The reaction was initiated by addition of ATP and samples were incubated under continuous light for 10 min at 30 °C. Incubation was terminated by adding 1 ml of 10% (w/v) trichloroacetic acid. The resulting precipitate was collected by centrifugation and washed 3–4 times with 1 ml of 10% trichloroacetic acid; the pellet was used for Cherenkov counting.

Crystallization of Rc^{2-190}—The protein was crystallized using the hanging-drop vapor diffusion method with a protein concentration of 30 mg/ml and the reservoir containing 2.4 M sodium malonate (pH 7.0) and 2 mM $CaCl_2$. This condition yielded plate-shaped crystals with a half-circle profile and a maximum diameter of 300–400 μm.

Data Collection—The x-ray diffraction dataset was collected at 100 K. Prior to cryocooling, crystals were step-soaked in reservoir solution containing 5–15% (v/v) glycerol.

Native data were recorded at beamline ID14–1 of the ESRF (Grenoble, France) tuned to a wavelength of 0.934 Å on an ADSC-Q4R detector. Because of the shape of the crystal, diffraction was extremely anisotropic, reducing the overall completeness of the dataset to ~85%. Data processing including reflections up to 3.0-Å resolution was carried out using MOSFLM (24) and SCALA, which is part of the CCP4 (25) software suite.

Structure Determination—Crystals of Rc^{2-190} belonged to space group $P2_1$. The structure was determined by molecular replacement using MOLREP (CCP4) with a single native dataset. The search model was created from the crystal structure of wild-type bovine recoverin (PDB code 1OMR, Ref. 22) by deleting residues 191–202. Crystals were found to contain four molecules per asymmetric unit, related by a proper 4-fold non-

TABLE 1
X-ray crystallographic data

Data collection	
Space group	$P2_1$
Cell dimensions	
a, b, c (Å, T = 100 K)	70.89, 70.76, 85.92
β (deg)	99.0
Resolution (Å)	70.0-3.0
Beamline	ESRF ID14-1
Detector	ADSC-Q4R
Wavelength (Å)	0.934
Unique reflections	14370
Average multiplicity	2.4 (2.2)[a]
Completeness (%)	84.8 (84.1)
R_{meas} (%)[b]	5.5 (29.6)
$\langle I \rangle / \sigma$ (I)	11.3 (1.7)
Refinement	
R_{work} (%)	23.7
R_{free} (%)[c]	25.9
Residue range	9–190
Number of atoms	
Protein	1439
Ions	1
Root mean square deviation	
Bond lengths (Å)	0.009
Bond angles (deg)	1.6

[a] Values in parentheses refer to the highest resolution shell (3.16-3.00 Å).
[b] $R_{meas} = \Sigma_h[N_h/(N_h-1)]^{1/2}\Sigma_i|I_{i,h}-\langle I_h \rangle|/\Sigma_h\Sigma_i I_{i,h}$, also termed redundancy-independent merging R factor ($R_{r.i.m.}$) (47) with $I_{i,h}$ representing the ith out of N_h measurements and $\langle I_h \rangle$ the mean of all observations of I_h.
[c] For calculation of R_{free}, 5% of all reflections were reserved.

crystallographic symmetry. Following rigid body refinement using the CNS package (26), the model was improved in an iterative manner including several cycles of positional refinement with CNS and manual rebuilding using O (27). In this process, strict non-crystallographic symmetry was applied throughout, *i.e.* all four molecules were assumed to be identical. For statistics on data collection and refinement refer to Table 1.

The final model comprises residues 9–190 of the protomer. According to Ramachandran plots generated with PROCHECK (CCP4), the model exhibits good geometry with none of the residues in the disallowed regions. The figures were generated with MOLSCRIPT (28) and RASTER3D (29) using secondary structure assignments given by the DSSP (30) program. The atomic coordinates and structure factors (code 2HET) have been deposited in the Protein Data Bank.

RESULTS

A truncated version of bovine recoverin lacking 12 amino acids at its C terminus (Rc^{2-190}) was heterologously expressed in *Escherichia coli* and purified to homogeneity from a bacterial cell extract. As expected, the purified protein showed an increased electrophoretic mobility in SDS-PAGE compared with the wild-type because of its lower molecular mass (not shown). Expression and purification of a myristoylated form of this mutant yielded preparations with the same high degree of purity. The extent of myristoylation was analyzed by reversed-phase HPLC and was found to be more than 95%. Furthermore, the myristoylated Rc^{2-190} could be easily distinguished from the non-myristoylated protein by its slightly higher electrophoretic mobility. Homogeneous preparations of myristoylated and non-myristoylated recoverin variants were used to determine some of their key biochemical properties. Non-myristoylated Rc^{2-190} was subjected to crystallization trials.

$^{45}Ca^{2+}$ Binding—The myristoylated form of Rc^{2-190} bound 2 Ca^{2+} ions in a cooperative manner, resembling the wild-type protein in this respect (Fig. 1*A*). However, the mutant showed a significantly lower affinity for Ca^{2+} indicated by a shift of the binding isotherm to higher free Ca^{2+} concentration; half-saturation was at 31.3 ± 4.2 μM for the mutant (three independent determinations) and 15.5 ± 2.1 μM for wild-type recoverin (two independent determinations). In the absence of the myristoyl group, the same principle observation was made, *i.e.* Rc^{2-190} bound Ca^{2+} with lower affinity and maximal stoichiometry was 2 Ca^{2+} per Rc^{2-190} (Fig. 1*B*). Binding of Ca^{2+} to the non-myristoylated mutant was non-cooperative, and data were fitted according to the two-site model as it has been previously applied to non-myristoylated wild-type recoverin (17). Interestingly, the low affinity EF-hand 2 of wild-type recoverin and of Rc^{2-190} display the same intrinsic affinity for Ca^{2+} (K_{d2} = 6.0 ± 0.2 μM), whereas the affinity of EF-hand 3 was more than 6-fold lower in Rc^{2-190} (K_{d1} = 1.4 ± 0.07 μM) than in wild-type recoverin (K_{d1} = 0.21 μM). These data show that EF-hands 2 and 3 are intact in the mutant, but that the C terminus influences the high affinity EF-hand 3.

Thermal Stability of Rc^{2-190}—To test whether the C-terminal truncation of recoverin might lead to a general destabilization of its structure, we compared the thermal stability of myristoylated wild-type recoverin and myristoylated Rc^{2-190} by recording the temperature dependence of tryptophan fluorescence in the presence and absence of Ca^{2+} (Fig. 1*C*). A change of the wavelength maximum of fluorescence emission (λ_{max}) at increasing temperature indicates thermal unfolding of the protein (13). Fluorescence emission of the mutant was slightly blue-shifted by 2 nm at temperatures below the transition point, which indicates small changes in the microenvironment of tryptophan residues caused by the removal of twelve C-terminal amino acids. At the same time, wild-type recoverin and the mutant Rc^{2-190} showed transitions from the folded to the unfolded state at the same temperature (Fig. 1*C*). For the Ca^{2+}-free forms, this transition occurred at lower temperature than for the Ca^{2+}-loaded forms indicating that the Ca^{2+}-loaded form of both recoverin variants is more stable. The overall thermal stability of the nonmyristoylated forms did not differ from the myristoylated forms; the λ_{max} was slightly more shifted in the case of Ca^{2+}-free recoverin, but the transition point was almost identical (not shown). These results demonstrate that the Rc^{2-190} mutant does not differ from wild-type recoverin in thermal stability. The changes in Ca^{2+}-affinity reported above do therefore not reflect a general destabilization of the mutant structure. However, we recognized that further shortening of the C terminus finally results in a thermally more unstable mutant, when more than 20 amino acids were deleted (data not shown).

Ca^{2+}-dependent Binding of Rc^{2-190} to Membranes—The change in the affinity for Ca^{2+} in myristoylated Rc^{2-190} suggested that the mutant should perform a Ca^{2+}-myristoyl switch with a shift in the Ca^{2+} dependence to higher free Ca^{2+} concentration. To test this assumption, we analyzed the binding of myristoylated recoverin forms to native washed ROS membranes by an equilibrium centrifugation assay. Binding of the mutant to ROS membranes showed a more than 2-fold shift to

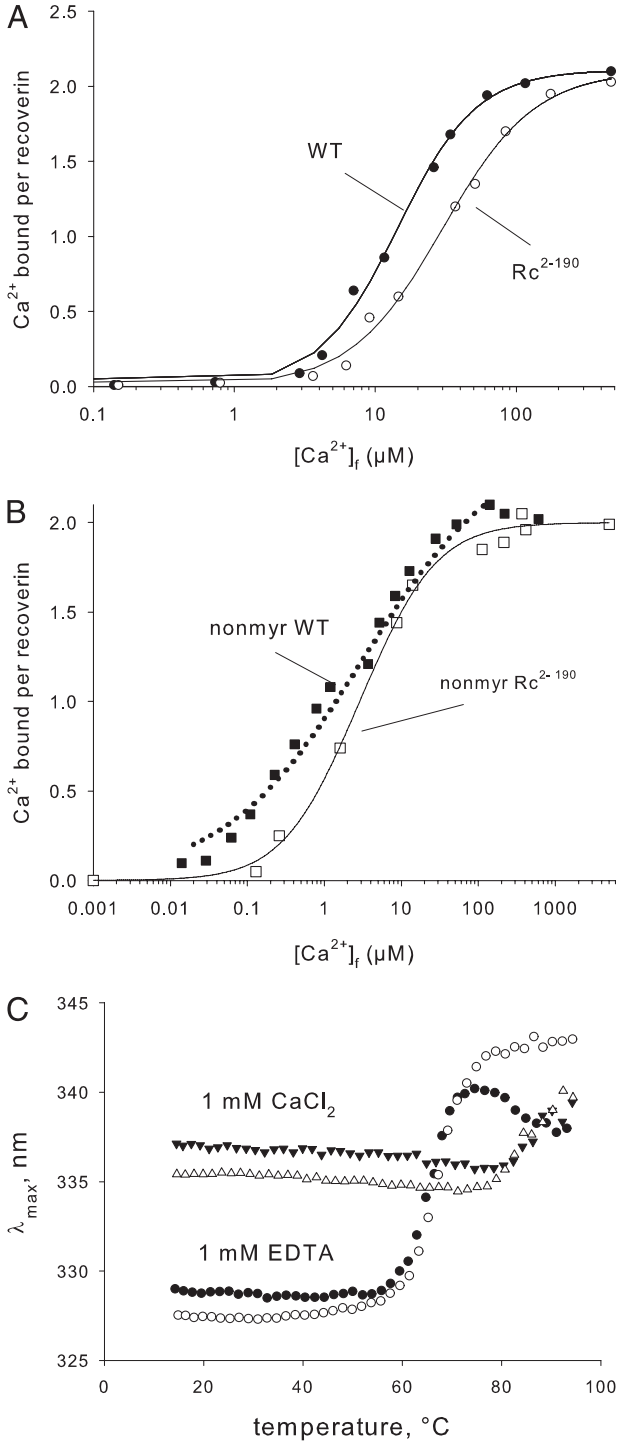

FIGURE 1. **$^{45}Ca^{2+}$ binding to wild-type recoverin and Rc^{2-190}.** *A*, myristoylated recoverin forms were incubated with increasing Ca^{2+} concentrations and the amount of bound Ca^{2+} was determined. *Solid lines* represent the best fit to the Hill model yielding for wild-type recoverin (●) EC_{50} = 14 μM, Hill coefficient n = 1.5 and for Rc^{2-190} (○) EC_{50} = 30 μM, n = 1.3. *B*, binding of $^{45}Ca^{2+}$ to non-myristoylated Rc^{2-190} (□). The *solid line* is a fit according to the two-site model yielding K_{d1} = 1.3 μM and K_{d2} = 6.2 μM. The *dotted line* represents a fit (two-site model) to published data (22) obtained with non-myristoylated wild-type recoverin (K_{d1} = 0.21 μM and K_{d2} = 6.2 μM) and (■) are data points of an independent control experiment using non-myristoylated wild-type recoverin. *C*, thermal stability of the recoverin forms. The maximum of tryptophan fluorescence emission was recorded for myristoylated wild-type recoverin (*filled symbols*) and myristoylated Rc^{2-190} (*open symbols*) at increasing temperature. Measurements were made in the presence of 1 mM $CaCl_2$ (*triangles*) or 1 mM EDTA (*circles*).

higher Ca^{2+} concentration, but finally reached the same maximal value as in the case of wild-type recoverin (Fig. 2*A*). In a second approach, we studied interaction of Rc^{2-190} with immobilized lipids using SPR spectroscopy (Fig. 2*B*). A lipid mixture that resembles the ROS disc membrane composition was immobilized on an L1 sensor chip. Injection of Rc^{2-190} onto the membrane surface in the presence of Ca^{2+} (*black bar*) caused an increase in resonance units indicating binding of Rc^{2-190} to the surface. Wild-type recoverin, however, bound to the same lipid surface with higher amplitude. If a decrease in Ca^{2+} affinity of Rc^{2-190} was responsible for this effect, the mutant should reach the same maximal amplitude as wild-type recoverin at higher Ca^{2+} concentration. Indeed, increasing the free Ca^{2+} concentration caused the SPR signal of the truncated mutant to converge to the wild-type level (Fig. 2*C*, see *dashed line*).

Inhibition of Rhodopsin Kinase—Recoverin is known to inhibit rhodopsin kinase activity at high Ca^{2+} concentration; this inhibitory effect is relieved when Ca^{2+} is lowered thereby allowing the kinase to phosphorylate its substrate rhodopsin. From the results concerning the modified Ca^{2+} sensitivity of Rc^{2-190} we predict that this mutant should be able to inhibit rhodopsin kinase, but with a shift in Ca^{2+} dependence of the dose-response curve. We tested this assumption by measuring the phosphorylation of rhodopsin by rhodopsin kinase in the presence of Rc^{2-190} or wild-type recoverin as a function of free Ca^{2+} (Fig. 3). Again, the truncated mutant exhibited a change in its Ca^{2+} sensitivity and inhibited rhodopsin kinase at higher Ca^{2+} concentration.

Crystal Structure of Rc^{2-190}—The above experiments demonstrated that truncation of the C-terminal 12 amino acids of recoverin affected its Ca^{2+} binding characteristics and, as a result, its Ca^{2+}-dependent biochemical properties such as performance of the Ca^{2+}-myristoyl switch and inhibition of rhodopsin kinase. In order to understand the molecular mechanisms underlying these functional alterations, we have crystallized the Rc^{2-190} mutant and determined its three-dimensional structure by x-ray crystallography. Rc^{2-190} forms plate-shaped crystals of space group $P2_1$ with four molecules per asymmetric unit. These are positioned in a head-to-tail fashion around a 4-fold non-crystallographic axis (perpendicular to the xy plane) resulting in a toroidal assembly encompassing a wide central channel (Fig. 4*A*). Crystallographic symmetry causes the tetramers to form layers parallel to the xy plane (two staggered layers per unit translation along z). This arrangement, which has not been observed before in crystal structures of NCS proteins, results in unique packing interactions, the structural implications of which are discussed below.

Crystallization of Rc^{2-190} was performed in the presence of 2 mM Ca^{2+}. While the electron density indicated the presence of a Ca^{2+} ion in EF-hand 3, the lower affinity EF-hand 2 turned out to be unoccupied. Therefore, like the crystal structure of wild-type recoverin (22), our structure of Rc^{2-190} represents an intermediate state resulting from Ca^{2+} binding to the high affinity EF-hand 3. The N-terminal 8 amino acids could not be located in the electron density and are thus likely to be disordered.

Superposition of the C_α traces of wild-type recoverin and the Rc^{2-190} mutant (Fig. 4*B*) reveals significant differences in sev-

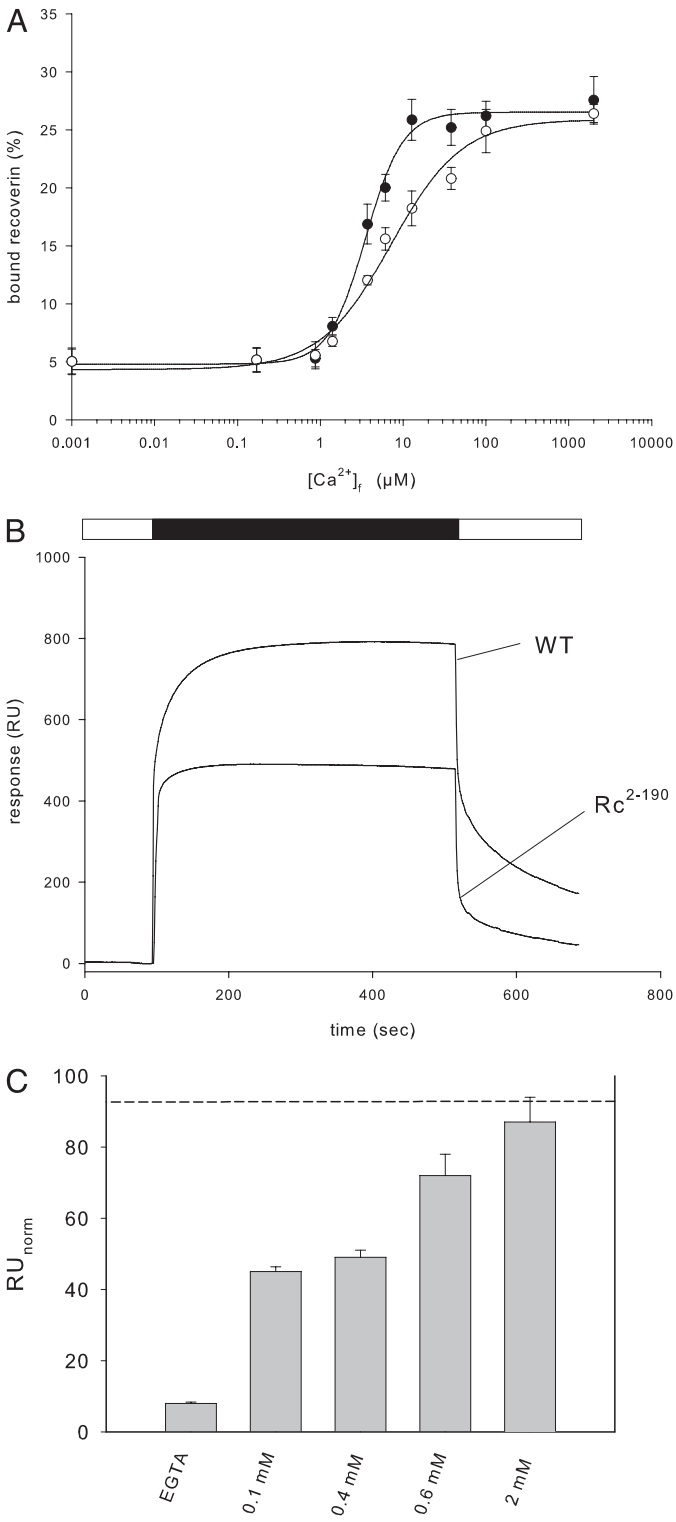

FIGURE 2. **Ca^{2+}-dependent binding of myristoylated recoverin forms to ROS membranes (*A*) and to immobilized lipids (*B*).** *A*, binding of wild-type recoverin (●) was half-maximal at 3 μM and binding of Rc^{2-190} (○) was half-maximal at 7 μM. *B*, SPR analysis of the interaction of wild-type recoverin and Rc^{2-190} with immobilized phospholipids. Recoverin forms were injected (*black bar*) into the SPR running buffer and time-dependent changes in resonance units (*RU*) were recorded as sensorgrams in the presence of 400 μM Ca^{2+}. Protein concentration was 30 μM. *C*, normalized amplitudes (RU_{norm}) of Rc^{2-190} binding to immobilized lipids analyzed by SPR spectroscopy. Recordings were made at increasing Ca^{2+} concentrations. The *dashed line* indicates the normalized amplitude obtained with wild-type recoverin.

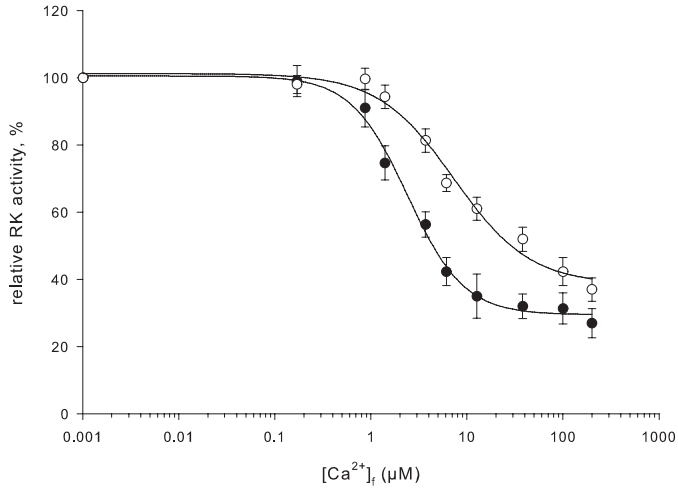

FIGURE 3. **Inhibition of rhodopsin kinase by myristoylated recoverin forms.** Rhodopsin kinase activity was measured by an *in vitro* phosphorylation assay as a function of free Ca^{2+}. Concentrations of wild-type recoverin (●) and Rc^{2-190} (○) were adjusted to 30 μM. *Solid lines* represent fits to the Hill model yielding for wild-type recoverin IC_{50} = 2.4 μM, n = 1.5, and for Rc^{2-190} IC_{50} = 7.3 μM, n = 1.1.

eral regions (highlighted in *red*). Generally, the C-terminal 12 amino acid truncation leads to increased flexibility in its neighborhood. This is particularly evident for the loop connecting the N- and C-terminal domains (region III), which is well-ordered in the wild-type protein. In contrast, the corresponding portion in the mutant not only adopts a different conformation, but also exhibits strongly enhanced mobility, indicated by large B factors[4] and very weak electron density. For a plot of main chain B factors per residue (normalized to the mean B value of all main chain atoms) please refer to Fig. 5.

Another part of the structure directly contacting the C terminus in the wild-type is the loop between EF-hands 3 and 4 (region IV, *colored orange* in Fig. 4*B*). Interestingly, the changes in average coordinates because of the truncation are rather modest in this segment. While relative main chain B factors in region IV are similar for both proteins, several side chains have become extremely mobile in the Rc^{2-190} mutant as judged from the lack of electron density in difference maps.

The conformation of the EF-hand 2 loop in Rc^{2-190} (region II) differs from the corresponding loop in the wild-type in that it is bent in the opposite direction and thus resembles the structure of the Ca^{2+}-occupied EF-hand 2 in myristoylated wild-type recoverin, as determined by NMR spectroscopy (15). However, because our x-ray structure of Rc^{2-190} does not contain a Ca^{2+} ion in EF-hand 2, this similarity is likely to be accidental, probably induced by the interaction of this loop with its non-crystallographic equivalent in an adjacent tetramer.

Another striking difference between the crystal structures of wild-type recoverin and the Rc^{2-190} mutant concerns the N-terminal α-helix and the loop connecting it to EF-hand 1 (region I). The helix is shifted in sequence (starting at Lys^{11}

[4] The B factor associated with an atom in a crystallographic model is proportional to the mean square displacement of this atom from its average position, assuming a simple harmonic motion. While also incorporating effects of static disorder and data quality, it is primarily taken as an indicator of thermal mobility.

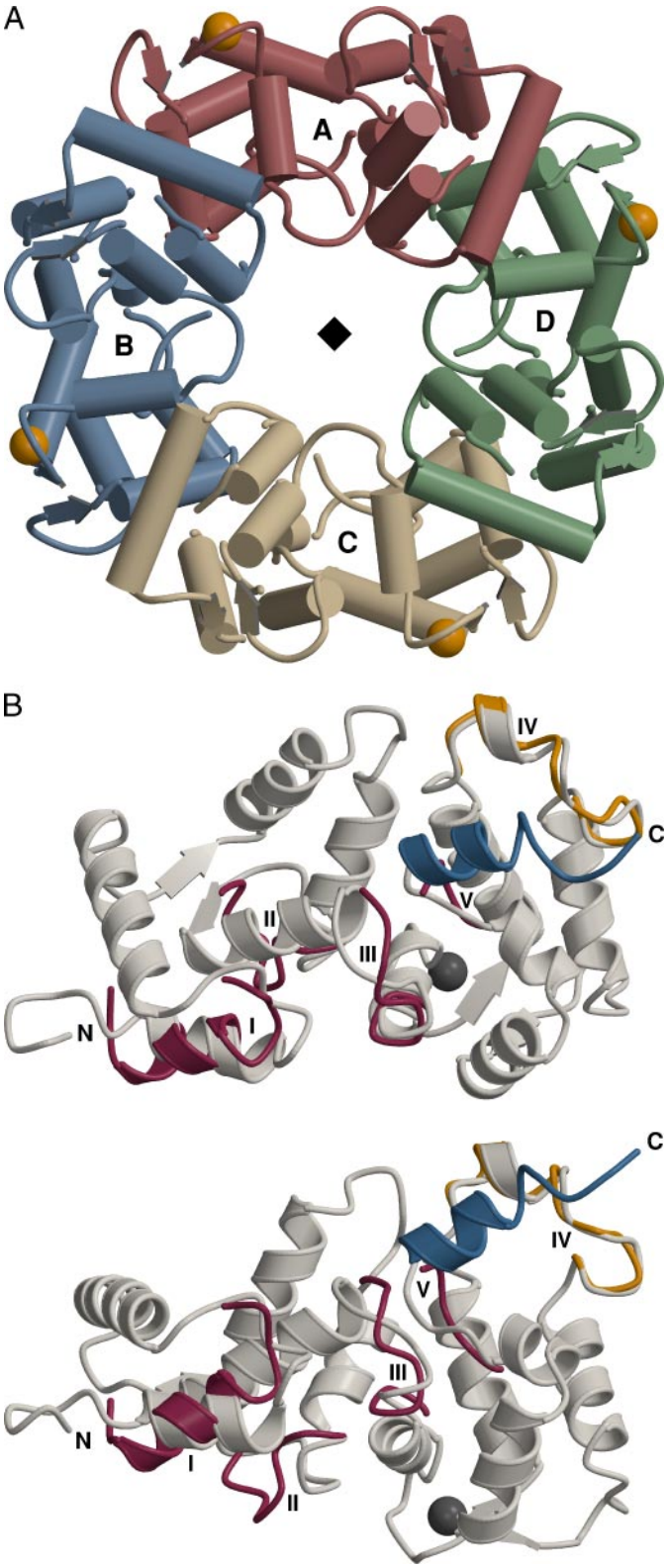

FIGURE 4. *A*, tetramer constituting the asymmetric unit of the Rc^{2-190} crystals described in this study. *Orange spheres* represent the Ca^{2+} ions bound to EF-hand 3 in each molecule. The position of the 4-fold non-crystallographic axis is indicated. *B*, segments in the crystal structure of Rc^{2-190} (shown in *red* or *orange* and numbered I through V) differing significantly from the wild-type (1OMR, *gray*). The C-terminal tail missing in the truncation mutant is shown in blue. Both views are related by a 45° rotation about the horizontal axis. See text for details.

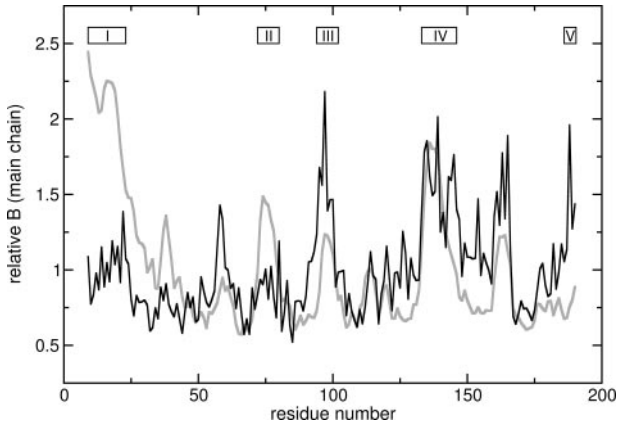

FIGURE 5. **Average main chain B factors per residue, normalized to the mean value of residues 9–190, for the crystal structures of the Rc^{2-190} mutant (*black*) compared with wild-type recoverin (1OMR, gray).** The numbering refers to the regions defined in Fig. 4.

instead of Leu^{9}) leading to an effective shortening of the subsequent loop. As a result, the helix is tilted by ~35° with respect to the wild type. These alterations may be partly due to a close interaction of the loop with a neighboring molecule in the same tetramer (such that Phe^{23} of molecule A, for example, contacts Leu^{102}, Ile^{173}, and Leu^{177} of molecule D). In addition, interactions between this loop and the domain linker, which are observed in the wild-type crystal structure, are completely lost in the truncation mutant because of the large gap between the two segments. The distance of C_α positions of Asn^{20} and Gly^{96}, for instance, increases from 5.8 Å in the wild type to 11.8 Å in the mutant. Despite the magnitude of the differences in this region their significance with respect to the truncation is unclear, so they will not be considered further.

DISCUSSION

The C-terminal segment of recoverin is unusual in that it contains a high fraction of basic side chains (six lysine residues within the dodecapeptide ^{191}QKVKEKLKEKKL^{202} in bovine recoverin). While the residues following Glu^{189} could not be resolved in the NMR structures of myristoylated recoverin (12, 15, 16), residues 190–196 form an α-helix in the crystal structure of the non-myristoylated protein (21, 22). The functional significance of this basic cluster has been subject to speculation. Matsuda *et al.* (19) compared the biological properties of the amphibian recoverin ortholog S-modulin and its cone paralog s26. Whereas S-modulin contains six basic residues in its C terminus, only two are present in the corresponding region of s26. The authors found that, at Ca^{2+} saturation, equilibrium binding to ROS membranes was significantly stronger for S-modulin than for s26. In both cases, binding was increased for the myristoylated compared with the non-myristoylated protein, but this effect was largely reversed with the addition of NaCl. From these data and further experiments using chimeric proteins and site-directed mutants they concluded that binding to ROS membranes and thus rhodopsin kinase inhibition may be modulated by an electrostatic interaction of the C-terminal portion of the recoverin homologs with membrane lipids. Recently, the orientation of myristoylated wild-type recoverin bound to membranes has been determined by solid state NMR

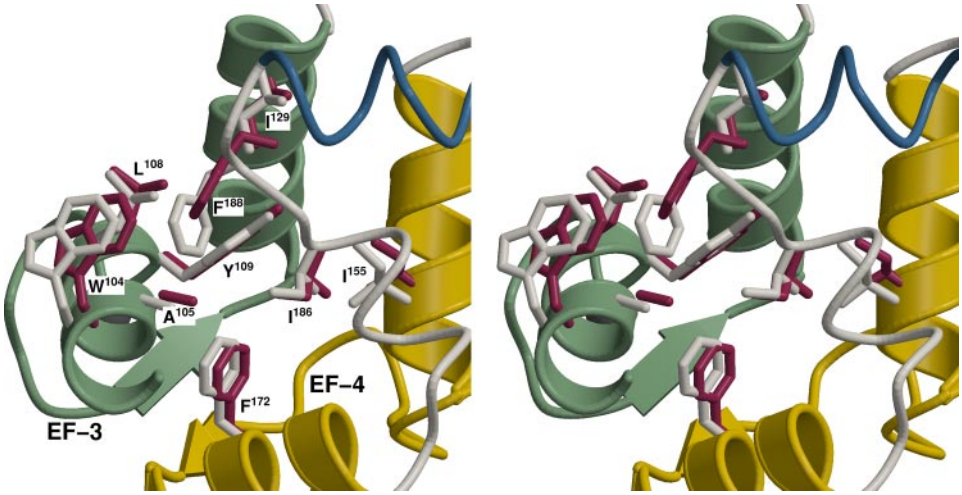

FIGURE 6. **Stereo representation showing the hydrophobic cluster linking Ile^{186} and Phe^{188} to apolar residues in EF-hand 3 (*green*) and EF-hand 4 (*yellow*).** The *ribbon backbone* is prepared from wild-type coordinates. Side chains of the wild-type protein are indicated in *gray*, those of the Rc$^{2-190}$ mutant in *red*. The most significant differences are observed for Phe^{188} and Trp^{104}.

spectroscopy (20). Because the myristoyl moiety is buried in the lipid bilayer and the long axis of the molecule is inclined by approx. 45° with respect to the membrane normal, the C terminus is positioned at a distance of more than 30 Å from the lipid surface. Electrostatic attraction involving this region is therefore very unlikely to play a significant role in membrane association by recoverin, at least in the myristoylated state.

In the present study, we address the role of the C-terminal segment for the structure and function of recoverin. Like the wild-type protein, the Rc$^{2-190}$ mutant has been crystallized in the presence of a large excess of Ca^{2+}, and both crystal structures contain a Ca^{2+} ion bound to EF-hand 3. Investigation of $^{45}Ca^{2+}$ binding to non-myristoylated Rc$^{2-190}$ revealed that the truncation changed the intrinsic Ca^{2+} affinity of EF-hand 3, whereas EF-hand 2 was unaffected (Fig. 1*B*). On the other hand, the cooperativity of Ca^{2+} binding is retained in the myristoylated mutant, leading to a shift of the entire binding isotherm toward higher free Ca^{2+} concentration (Fig. 1*A*).

It should be noted that a comprehensive evaluation of the significance of the C-terminal segment would require structural data on the Ca^{2+}-free and Ca^{2+}-bound forms of both the wild-type and the truncated protein. Unfortunately, crystals of non-myristoylated recoverin are available only for the intermediate states with Ca^{2+} bound to EF-hand 3. On the other hand, because of the lack of cooperativity in Ca^{2+} binding to the non-myristoylated variants, the C-terminal domains of our crystal structures with occupied EF-hand 3 should be representative of the respective Ca^{2+}-saturated forms, irrespective of the myristoylation state. We confirmed this (22) for wild-type recoverin and for a mutant with a disabled EF-hand 2 (E85Q), for which solution structures are available (15, 20), so it is likely to hold for Rc$^{2-190}$ as well. In the x-ray structure of the wild-type, the C-terminal α-helix (alternatively designated helix K) contacts and stabilizes the loop connecting EF-hands 3 and 4. This is accomplished by hydrophobic contacts (Val^{193}-Ile^{133} and Leu^{197}-Leu^{141}) as well as electrostatic interactions between ^{194}K*XXXX*K^{198} and ^{136}ED^{137}. Interestingly, the remaining four lysine side chains in the C-terminal segment form contacts with acidic residues neighboring in sequence but do not interact with other parts of the protein.

The loop immediately preceding the C-terminal helix (residues 186–190) is of particular interest with respect to the truncation. While constituting the new C terminus in the Rc$^{2-190}$ mutant, this segment still adopts a central position in the molecule and contributes to the hydrophobic core (Fig. 6). Specifically, Phe^{188} directly contacts Trp^{104}, Ala^{105}, and Leu^{108} in the entering helix as well as Ile^{129} in the exiting helix of EF-hand 3, whereas Ile^{186} interacts with Tyr^{109} from the EF-hand 3 entering helix and Ile^{155} and Phe^{172} from the entering and exiting helices, respectively, of EF-hand 4. The B factor plot in Fig. 5 reveals strongly increased flexibility at the C terminus of the Rc$^{2-190}$ mutant. Because of the hydrophobic network outlined above, elevated thermal motion should also be noticeable in other parts of the C-terminal domain. Indeed, the ratio of average main chain B factors of the N-terminal (residues 9–94) and C-terminal domains (residues 102–190) is reversed in the mutant (0.79) with respect to wild-type recoverin (1.25), indicating that the truncation induces a general increase in conformational mobility throughout the C-terminal domain of recoverin.

How do these structural alterations relate to the changes in Ca^{2+} affinity observed for the Rc$^{2-190}$ mutant? Ca^{2+} binding to EF-hand structures is known to be associated with characteristic conformational changes. These are not confined to the dodecamer loop containing the ion-coordinating residues but also involve the adjacent helices, which perform a combination of rotation, translation, and tilting motions (31). Moreover, we have recently presented experimental evidence that EF-hands 3 and 4 of recoverin are conformationally coupled to one another (32). The molecular mechanics of this complex structural transition are closely related to the difference in free energy between the Ca^{2+}-free and Ca^{2+}-bound states, which ultimately determines the apparent Ca^{2+} affinity of the molecule. Although definition of a precise chain of cause and effect is not warranted by our data, the observation of increased thermal mobility in the C-terminal domain suggests that, in addition to changes in the average structure, the truncation alters the conformational dynamics of the protein. We speculate that this will interfere with the coordinated movements of the EF-hand helices associated with Ca^{2+} binding (see above) and thus impair Ca^{2+} binding itself.

We therefore propose a novel role for the C-terminal helical segment of recoverin as a built-in affinity modulator.[5] This

[5] In the case of recoverin, there is currently no experimental evidence for a regulatory mechanism targeting the C-terminal segment *in vivo*, although its intrinsic mobility would be compatible with such a function (see below). The term "affinity modulator" therefore refers to the truncated mutant and to related proteins lacking this part of the structure.

function involves interference with conformational changes associated with Ca^{2+} binding rather than influence on the coordination sites themselves, and in this respect resembles the role of the N-terminal myristoyl moiety. However, we note several important differences: First, the two effectors, the myristoyl group and the C-terminal helical segment, primarily act on different domains of the protein. Second, the myristoyl chain stablizes the T-state of recoverin, whereas the C-terminal helix increases the R-state probability. And finally, induction of cooperativity of Ca^{2+} binding is a unique property of the N-terminal acylation.

The physiological role of recoverin as a Ca^{2+}-dependent regulator of rhodopsin kinase has been extensively discussed in previous publications (Refs. 8 and 9 and references therein). While there is a general agreement that recoverin regulates the activity of rhodopsin kinase *in vitro*, the main argument against an *in vivo* operation on rhodopsin kinase activity comes from the mismatch of the Ca^{2+} dependence of rhodopsin kinase inhibition (Fig. 3) and the change in cytoplasmic Ca^{2+} from 250 nM in darkness to 20 nM after illumination observed for example in mice rods (33). However, Klenchin *et al.* (34) showed that the Ca^{2+}-dependent regulation of rhodopsin kinase is shifted into the physiological range, when the *in vitro* data are extrapolated to the *in vivo* conditions by a mass action calculation. In addition, recoverin-deficient mice exhibit a shortened photoresponse, which is consistent with an action of recoverin on rhodopsin kinase activity (35). Finally, we recently showed that recoverin is present in detergent resistant membranes even in the absence of Ca^{2+}. The high cholesterol content of these membranes facilitates membrane binding of recoverin and can shift its Ca^{2+}-dependent properties to lower free Ca^{2+} concentration, *i.e.* into the physiologically relevant range (36). Thus, cholesterol appears as an additional external modulator of Ca^{2+} sensitivity. Notably, recent publications indicate that recoverin might have additional functions: for instance, it undergoes a light-dependent intracellular translocation to rod synaptic terminals (37) and enhances the signal transfer between rods and rod bipolar cells in mouse retina by an unknown mechanism (38).

Three-dimensional structures are available for several members of the neuronal calcium sensor family. In addition to recoverin, these include NMR structures of yeast frequenin (39) and bovine GCAP-2 (40) as well as crystal structures of human NCS-1 (41), bovine neurocalcin δ (42), and human potassium channel interacting protein (KChIP)-1 (43). Among these structures, the C-terminal α-helix has been observed exclusively in the crystal structures of recoverin, whereas in other cases this segment was either disordered or even absent in the primary sequence. The latter is exemplified by frequenin (NCS-1), which consists of only 190 amino acids and may be regarded as a naturally occurring analog of our truncated Rc^{2-190} mutant.

Helical extensions C-terminal to EF-hand 4 have also been observed in the structures of related EF-hand proteins not belonging to the NCS family, such as human calcineurin (CN) B (44) and calcineurin B-like protein (CBL) 2 from *A. thaliana* (45). In the CNA-CNB complex, an α-helix of CNA is bound in a large hydrophobic crevice extending over both domains of CNB. Exposure of hydrophobic residues upon Ca^{2+} binding is a common feature of EF-hand motifs and results from the "opening" movement of the helix pair, the extent of which varies considerably between individual proteins. In the CNB and CBL2 structures, the hydrophobic patch exposed on the C-terminal domain is shielded by helices J and (in the case of CBL2) K, but in the CNB-CNA complex this segment is displaced by the interacting CNA helix (44). A similar mechanism has been suggested for the interaction of CBL2 with its target CIPK (CBL-interacting protein kinase), which is mediated by a hydrophobic stretch in the CIKP sequence (45).

Based on biochemical and molecular biological data, NCS proteins are generally believed to interact with their targets via an apolar surface on the N-terminal domain, whereas the analogous hydrophobic patch on the C-terminal domain is largely covered by helix J. An exception is found in the crystal structure of human NCS-1 (41) which displays an extended hydrophobic groove because of a lateral displacement of helix J. By contrast, in the solution structure of its yeast homolog frequenin, helix J is found in the canonical position. This discrepancy is likely to indicate a conformational transition intrinsic to this protein, with the NMR data representing the predominant conformation in solution and the x-ray structure containing a conformer most favored by crystal packing interactions. While the significance of this observation for NCS-1 function is presently unclear, the striking similarity with the conformational switch in CNB suggests that this mechanism of target recognition might be an ancient feature of EF-hand proteins. As a result of the intriguing competition between intramolecular and intermolecular interactions, the hydrophobic surface, which might destabilize the protein when solvent-exposed, would be uncovered only if demanded by the binding partner.

Because other NCS proteins probably have evolved from a frequenin-like ancestor, we speculate that they might have retained some aspects of this mechanism of target interaction. In addition to rhodopsin kinase, Ca^{2+}-loaded recoverin, for instance, may bind other proteins at the disc membrane or in the cytoplasm of the photoreceptor, possibly involving interaction sites on the C-terminal domain.

Our results tackle a fundamental problem in understanding the molecular basis of NCS protein function, *i.e.* how to explain the enormous functional diversity of NCS proteins (including different Ca^{2+} sensitivities) in light of the striking similarities in their three-dimensional structures. Here we show how fine-tuning of crucial regulatory properties can be achieved by a short polypeptide segment. During evolution, certain subclasses of NCS proteins may have faced the need to modify, or possibly disable, the ancient mechanism of target recognition via the C-terminal domain. We propose that distinctive structural features like the terminal helix K in recoverin may have played an important role in the process of diversification of NCS proteins, since they can serve to modify both the Ca^{2+} binding properties and the exposure of interaction surfaces. On the other hand, NCS proteins might display a similar conformational plasticity (46) as calmodulin while forming complexes with their targets.

Acknowledgments—We thank Georg Büldt for continuous generous support. Furthermore, assistance by the technical staff at beamline ID14-1 of the ESRF (Grenoble, France), is acknowledged.

REFERENCES

1. Rizo, J., and Südhof, T. C. (1998) *J. Biol. Chem.* **273,** 15879–15882
2. Lewit-Bentley, A., and Réty, S. (2000) *Curr. Opin. Struct. Biol.* **10,** 637–643
3. Braunewell, K. H., and Gundelfinger, E. D. (1999) *Cell Tissue Res.* **295,** 1–12
4. Burgoyne, R. D., O'Callaghan, D. W., Hasdemir, B., Haynes, L. P., and Tepikin, A. V. (2004) *Trends Neurosci.* **27,** 203–209
5. Palczewski, K., Polans, A. S., Baehr, W., and Ames, J. B. (2000) *Bioessays* **22,** 337–350
6. Kawamura, S., Hisatomi, O., Kayada, S., Tokunaga, F., and Kuo, C. H. (1993) *J. Biol. Chem.* **268,** 14579–14582
7. Gorodovikova, E. N., Senin, I. I., and Philippov, P. P. (1994) *FEBS Lett.* **353,** 171–172
8. Erickson, M. A., Lagnado, L., Zozulya, S., Neubert, T. A., Stryer, L., and Baylor, D. A. (1998) *Proc. Natl. Acad. Sci. U. S. A.* **95,** 6474–6479
9. Senin, I. I., Koch, K.-W., Akhtar, M., and Philippov, P. P. (2002) *Adv. Exp. Med. Biol.* **514,** 69–99
10. Burns, M. E., and Baylor, D. A. (2001) *Annu. Rev. Neurosci.* **24,** 779–805
11. Dizhoor, A. M., Ericsson, L. H., Johnson, R. S., Kumar, S., Olshevskaya, E., Zozulya, S., Neubert, T. A., Stryer, L., Hurley, J. B., and Walsh, K. A. (1992) *J. Biol. Chem.* **267,** 16033–16036
12. Tanaka, T., Ames, J. B., Harvey, T. S., Stryer, L., and Ikura, M. (1995) *Nature* **376,** 444–447
13. Permyakov, S. E., Cherskaya, A. M., Senin, I. I., Zargarov, A. A., Shulga-Morskoy, S. V., Alekseev, A. M., Zinchenko, D. V., Lipkin, V. M., Philippov, P. P., Uversky, V. N., and Permyakov, E. A. (2000) *Protein Eng.* **13,** 783–790
14. Zozulya, S., and Stryer, L. (1992) *Proc. Natl. Acad. Sci. U. S. A.* **89,** 11569–11573
15. Ames, J. B., Ishima, R., Tanaka, T., Gordon, J. I., Stryer, L., and Ikura, M. (1997) *Nature* **389,** 198–202
16. Ames, J. B., Hamasaki, N., and Molchanova, T. (2002) *Biochemistry* **41,** 5776–5787
17. Senin, I. I., Fischer, T., Komolov, K. E., Zinchenko, D. V., Philippov, P. P., and Koch, K.-W. (2002) *J. Biol. Chem.* **277,** 50365–50372
18. Lange, C., and Koch, K.-W. (1997) *Biochemistry* **36,** 12019–12026
19. Matsuda, S., Hisatomi, O., and Tokunaga, F. (1999) *Biochemistry* **38,** 1310–1315
20. Valentine, K. G., Mesleh, M. F., Opella, S. J., Ikura, M., and Ames, J. B. (2003) *Biochemistry* **42,** 6333–6340
21. Flaherty, K. M., Zozulya, S., Stryer, L., and McKay, D. B. (1993) *Cell* **75,** 709–716
22. Weiergräber, O. H., Senin, I. I., Philippov, P. P., Granzin, J., and Koch, K.-W. (2003) *J. Biol. Chem.* **278,** 22972–22979
23. Neubert, T. A., Walsh, K. A., Hurley, J. B., and Johnson, R. S. (1997) *Protein Sci.*, **6,** 843–850
24. Leslie, A. G. W. (1992) *Jnt. CCP4/ESF-EAMCB Newslett. Protein Crystallogr.* **26,**
25. Collaborative computational project, Number 4 (1994) *Acta Crystallogr.* **D50,** 760–763
26. Brünger, A. T., Adams, P. D., Clore, G. M., Delano, W. L., Gros, P., Grosse-Kunstleve, R. W., Jiang, J.-S., Kuszewski, J., Nilges, N., Pannu, N. S., Read, R. J., Rice, L. M., Simonson, T., and Warren, G. L. (1998) *Acta Crystallogr.* **D54,** 905–921
27. Jones, T. A., Zou, J.-Y., Cowan, S. W., and Kjeldgaard, M. (1991) *Acta Crystallogr.* **A47,** 110–119
28. Kraulis, P. J. (1991) *J. Appl. Crystallogr.* **24,** 946–950
29. Merritt, E. A., and Bacon, D. J. (1997) *Methods Enzymol.* **277,** 505–524
30. Kabsch, W., and Sander, C. (1983) *Biopolymers* **22,** 2577–2637
31. Yap, K. L., Ames, J. B., Swindells, M. B., and Ikura, M. (1999) *Proteins: Struct. Funct. Genet.* **37,** 499–507
32. Senin, I. I., Vaganova, S. A., Weiergräber, O. H., Ergorov, N. S., Philippov, P. P., and Koch, K.-W. (2003) *J. Mol. Biol.* **330,** 409–418
33. Woodruff, M. L., Sampath, A. P., Matthews, H. R., Krasnoperova, N. V., Lem, J., and Fain, G. L. (2002) *J. Physiol.* **542,** 843–854
34. Klenchin, V. A., Calvert, P. D., and Bownds, M. D. (1995) *J. Biol. Chem.* **270,** 16147–16152
35. Makino, C. L., Dodd, R. L., Chen, J., Burns, M. E., Roca, A., Simon, M. I., and Baylor, D. A. (2004) *J. Gen. Physiol.* **123,** 729–741
36. Senin, I. I., Hoeppner-Heitmann, D., Polkovnikova, O. O., Churumova, V. A., Tikhomirova, N. K., Philippov, P. P., and Koch, K.-W. (2004) *J. Biol. Chem.* **279,** 48647–48653
37. Strissel, K. J., Lishko, P. V., Trieu, L. H., Kennedy, M. J., Hurley, J. B., and Arshavsky, V. Y. (2005) *J. Biol. Chem.* **280,** 29250–29255
38. Sampath, A. P., Strissel, K. J., Elias, R., Arshavsky, V., McGinnis, J. F., Chen, J., Kawamura, S., Rieke, F., and Hurley, J. B. (2005) *Neuron* **46,** 413–420
39. Ames, J. B., Hendricks, K. B., Strahl, T., Huttner, I. G., Hamasaki, N., and Thorner, J. (2000) *Biochemistry* **39,** 12149–12161
40. Ames, J. B., Dizhoor, A. M., Ikura, M., Palczewski, K., and Stryer, L. (1999) *J. Biol. Chem.* **274,** 19329–19337
41. Bourne, Y., Dannenberg, J., Pollmann, V., Marchot, P., and Pongs, O. (2001) *J. Biol. Chem.* **276,** 11949–11955
42. Vijay-Kumar, S., and Kumar, V. D. (1999) *Nat. Struct. Biol.* **6,** 80–88
43. Scannevin, R. H., Wang, K., Jow, F., Megules, J., Kopsco, D. C., Edris, W., Carroll, K. C., Lu, Q., Xu, W., Xu, Z., Katz, A. H., Olland, S., Lin, L., Taylor, M., Stahl, M., Malakian, K., Somers, W., Mosyak, L., Bowlby, M. R., Chanda, P., and Rhodes, K. J. (2004) *Neuron* **41,** 587–598
44. Kissinger, C. R., Parge, H. E., Knighton, D. R., Lewis, C. T., Pelletier, L. A., Tempczyk, A., Kalish, V. J., Tucker, K. D., Showalter, R. E., Moomaw, E. W., Gastinel, L. N., Habuka, N., Chen, X., Maldonado, F., Barker, J. E., Bacquet, R., and Villafranca, J. E. (1995) *Nature* **378,** 641–644
45. Nagae, M., Nozawa, A., Koizumi, N., Sano, H., Hashimoto, H., Sato, M., and Shimizu, T. (2003) *J. Biol. Chem.* **278,** 42240–42246
46. Ikura, M., and Ames, J. B. (2006) *Proc. Natl. Acad. Sci. U. S. A.* **103,** 1159–1164
47. Diederichs, K., and Karplus, P. A. (1997) *Nat. Struct. Biol.* **4,** 269–275